J. Anat. (1998) **192**, pp. 517–528, with 6 figures Printed in the United Kingdom

Spatial distribution of nerve processes and β-adrenoreceptors in the rat atrioventricular node

KEVIN PETRECCA AND ALVIN SHRIER

Department of Physiology, McGill University, Montréal, Québec, Canada

(*Accepted 17 February 1988*)

ABSTRACT

Atrioventricular (AV) nodal conduction time is known to be modulated by the autonomic nervous system. The presence of numerous parasympathetic and sympathetic nerve fibres in association with conduction tissue in the heart is well authenticated. In this study, confocal microscopy was used to image the distribution of antibodies directed against the general neuronal marker PGP 9.5, tyrosine hydroxylase (TH), vasoactive intestinal peptide (VIP), calcitonin gene-related peptide (CGRP) and β_1 and β_2-adrenoreceptors. Serial 12 μm sections of fresh frozen tissue taken from the frontal plane of the rat atrioventricular node, His bundle and bundle branches were processed for histology, acetylcholinesterase (AChE) activity and immunohistochemistry. It was found that the AV and ventricular conduction systems were more densely innervated than the atrial and ventricular myocardium as revealed by PGP 9.5 immunoreactivity. Furthermore, the transitional cell region was more densely innervated than the midnodal cell region, while spatial distribution of total innervation was uniform throughout all AV nodal regions. AChE-reactive nerve processes were found throughout the AV and ventricular conduction systems, the spatial distribution of which was nonuniform exhibiting a paucity of AChE-reactive nerve processes in the central midnodal cell region and a preponderance in the circumferential transitional cell region. TH-immunoreactivity was uniformly distributed throughout the AV and ventricular conduction systems including the central midnodal and circumferential transitional cell regions. β_1-adrenoreceptors were found throughout the AV and ventricular conduction systems with a preponderance in the circumferential transitional cell region. β_2-adrenoreceptors were localised predominantly in AV and ventricular conduction systems with a paucity of expression in the circumferential transitional cell region. These results demonstrate that the overall uniform distribution of total nerve processes is comprised of nonuniformly distributed subpopulations of parasympathetic and sympathetic nerve processes. The observation that the midnodal cell region exhibits a differential spatial pattern of parasympathetic and sympathetic innervation suggests multiple sites for modulation of impulse conduction within this region. Moreover, the localisation of β_2-ARs in the AV conduction system, with an absence of expression in the circumferential transitional cell layer, suggests that subtype-specific pharmacological agents may have distinct effects upon AV nodal conduction.

Key words: Heart; cardiac conducting system; autonomic nervous system.

INTRODUCTION

The cardiac electrical impulse is initiated at the sinoatrial (SA) node, propagates through the atrial myocardium to the atrioventricular (AV) node and ultimately passes through the ventricular conduction system. The AV node, a complex structure composed of a number of regions containing distinct cell types (Anderson, 1972), functions to delay and regulate impulse conduction between the atria and ventricles. Cells in the region of the AV node (atrionodal (AN), nodal (N), and nodal-His (NH)) are characterised by a variety of action potential configurations and a range of upstroke velocities (Paes de Carvalho & Almeida, 1960; Billette, 1987; Munk et al. 1996).

It is well known that AV nodal conduction time is influenced by the autonomic nervous system (ANS). Parasympathetic stimulation results in an increase in

Correspondence to Dr Alvin Shrier, Department of Physiology, McGill University, 3655 Drummond Street, Montréal, Québec, Canada H3G 1Y6. Tel: +1 514 398 4318; fax: +1 514 398 7452; e-mail: ashrier@physio.mcgill.ca.

the P-R interval while sympathetic stimulation results in a decrease (Hoffman, 1967; Levy & Martin, 1979). The presence of numerous parasympathetic and sympathetic nerve processes in association with conduction tissue in the heart is well authenticated (Anderson, 1972; Mochet et al. 1975), supporting the concept of neural control of conduction.

In addition to the classical neurotransmitters, acetylcholine (ACh) and noradrenaline (NA), recent studies have shown that a number of neuropeptides (e.g. vasoactive intestinal peptide (VIP), calcitonin gene-related peptide (CGRP)) are released from nerve terminals in the heart, along with these classical neurotransmitters, exerting variable cardiovascular effects (Fisher et al. 1983; Rigel & Lathrop, 1990; Hill et al. 1993).

In addition, β-adrenoreceptors (β-ARs), which mediate the actions of catecholamines, have also been reported to play important roles in the conduction system of the heart. β_1 and β_2-ARs have been shown to be expressed at high levels in human and dog SA nodes (Beau et al. 1995; Rodefeld et al. 1996) and rat and guinea pig AV nodes (Saito et al. 1998; Molenaar et al. 1990). These autoradiographic studies, however, have not allowed for a precise determination of the spatial distribution of these receptors.

In the present study we have used histological, histochemical and immunohistochemical techniques to determine the spatial distribution of the parasympathetic and sympathetic innervation in the rat AV node, His bundle and bundle branches. Acetylcholinesterase (AChE) was used as a marker for parasympathetic nerve processes and tyrosine hydroxylase (TH) was used as a marker for sympathetic nerve processes. In addition, the localisation of the neuropeptides, VIP and CGRP, and β-ARs, β_1 and β_2, was also determined.

METHODS

Tissue processing

14 adult Sprague-Dawley rats (150–250 g) were killed by cervical dislocation. A midline thoracotomy was performed and the heart was rapidly removed and dissected. The preparation, containing most of the right atrium, the interatrial septum, the atrioventricular region, the annulus fibrosus, and the upper portion of the interventricular septum, was placed in a tissue bath and pinned in its proper orientation while being perfused with Tyrode solution (composition (mM): 121 NaCl, 5 KCl, 15 $NaHCO_3$, 1 Na_2HPO_4, 2.8 Na acetate, 1 $MgCl_2$, 2.2 $CaCl_2$ and 5.5 glucose) and gassed with a 95% O_2 and 5% CO_2 mixture. Temperature was maintained at 37.0 °C and the pH was 7.4. This procedure required approximately 30–60 s. Thereafter, the preparation was immediately frozen in isopentane previously cooled to −40 °C, then trimmed into a small block containing the interatrial septum, the upper portion of the interventricular septum, and the ostium of the coronary sinus. The blocks were oriented to allow sectioning at right angles to the annulus fibrosus in the frontal plane, mounted on a cryostat tissue holder using Histo Prep (Fisher Scientific, Ontario, Canada), placed on the rapid-freeze stage of a Microm cryostat (Carl Zeiss) and the entire AV node, His bundle and proximal bundle branches were cut into 12 μm sections. Every section was collected and processed for histological, acetylcholinesterase or immunohistochemical staining.

Histology

All sections were collected on glass slides and, after drying at room temperature (20–22 °C), incubated in Bouin's solutions for 10 min at 60 °C. Sections were subsequently rinsed in running tap water and stained using a modified Masson's trichrome technique. Sections were washed in 1% acetic acid for 2 min and dehydrated in increasing concentrations of alcohol and ultimately cleared in xylene and mounted. Sections were examined using a light microscope and photographed using Kodak film. Red staining indicates myocardial cells and blue staining indicates connective tissue.

Acetylcholinesterase staining

The localisation of AChE activity was investigated by a method previously described by El-Badawi & Schenk (1967). Briefly, fresh-frozen 12 μm cryostat sections were rinsed in acetate buffer (0.1 M, pH 6.0) and subsequently immersed in the incubation medium at a 30-fold higher dilution than was originally described. After rinsing in Tris-hydrochloride (50 mM, pH 7.6), AChE activity was visualised by immersion of the sections for 5 min in Tris hydrochloride buffer (50 mM, pH 7.6) containing 0.04% 3,3′-diaminobenzidine tetrahydrochloride and 0.03% nickel ammonium sulphate and then for a further 3–5 min with the addition of 0.003% hydrogen peroxide.

In control experiments, AChE activity could not be detected after incubation of sections in the absence of acetylthiocholine iodide or after the addition of

Table. *Source and characterisation of primary and secondary antisera*

Antigen	Host species	Code	Source
PGP-9.5	Mouse	UC 13C4	Accurate Chemical & Scientific Corporation
TH	Mouse	1 017 381	Boehringer Mannheim
β_1-AR	Rabbit	sc-568	Santa Cruz Biotechnology, Inc.
β_2-AR	Rabbit	sc-570	Santa Cruz Biotechnology, Inc.
VIP	Guinea-pig	BGP 341-100	Accurate Chemical & Scientific Corporation
CGRP	Guinea pig	BGP 470-100	Accurate Chemical & Scientific Corporation
Mouse IgG	Goat	115-095-100	Jackson ImmunoResearch Laboratories, Inc.
Rabbit IgG	Goat	111-095-144	Jackson ImmunoResearch Laboratories, Inc.
Guinea pig IgG	Goat	02-17-06	Kirkegaard & Perry Laboratories, Inc.

PGP-9.5, protein gene product-9.5; TH, tyrosine hydroxylase; β_1-AR, β_1-adrenergic receptor; β_2-AR, β_2-adrenergic receptor; VIP, vasoactive intestinal polypeptide; CGRP, calcitonin gene-related peptide.

10^{-4} mol/l eserine (physostigmine, Sigma Chemical Co., USA) to the incubation medium. Sections were examined using a light microscope and photographed using Kodak film.

Antibodies

The source and characterisation of the antibodies used is given in the Table.

Immunohistochemistry

An indirect immunofluorescence technique was used together with specific primary antisera to the general neuronal marker PGP-9.5, tyrosine hydroxylase (TH), β_1-ARs, β_2-ARs, VIP and CGRP (Table). Briefly, 12 μm cryostat sections, prepared from fresh-frozen tissue, were air-dried at room temperature (20–22 °C). Sections immunolabelled with anti-VIP and anti-CGRP antibodies were incubated in a 3% paraformaldehyde/sodium-phosphate buffer solution for 30 min at room temperature and subsequently rinsed in phosphate buffered saline (PBS). All other immunolabelling was performed on unfixed tissue. All sections were then incubated for 30 min in PBS containing 0.2% Triton X-100. After 3 rinses in PBS, sections were stained with Pontamine sky blue (BDH, England) for 30 min in order to reduce tissue autofluorescence (Cowen et al. 1985). Sections were subsequently rinsed and incubated for 3 h at room temperature in appropriately diluted primary antisera followed by 3 10 min rinses. Sections were then incubated for 1.5 h at room temperature in appropriately diluted secondary antisera; fluorescein isothiocyante (FITC)-conjugated goat antimouse IgG, FITC-conjugated goat antirabbit IgG or FITC-conjugated goat antiguinea pig IgG. These incubations were followed by 3 10 min rinses. The preparations were mounted with Immuno Fluore (ICN, Canada).

Specificity controls included omission of primary antisera and preabsorption of anti-TH with tyrosine hydroxylase (Sigma, Ontario, Canada), anti-β_1-AR and anti-β_2-AR with their corresponding control peptides (Santa Cruz Biotechnology, USA), and anti-VIP and anti-CGRP with their corresponding control peptides (Peninsula Laboratories, USA).

All imaging was performed using a Zeiss LSM 410 inverted confocal microscope. FITC-conjugated secondary antibodies were imaged by exciting the sample with a 488 nm line from an argon/krypton laser and the resulting fluorescence was collected on a photomultiplier after passage through FT510 and BP515-540 filter sets. Optical sections were taken using a $\times 25$, 0.8 NA (optical thickness = 3.1 μm) objective or a $\times 63$, 1.4 NA objective (optical thickness = 1.0 μm). All images were printed on a Kodak XLS8300 high resolution (300 DPI) printer.

RESULTS

All tissue sections shown in this study are serial sections taken from the same heart. Furthermore, the findings from this heart, including all AChE reactivity and immunohistochemical data, are completely consistent with those found in the 13 other hearts that were examined.

Morphology

The AV node is situated anterior to the ostium of the coronary sinus and posterior to the membranous

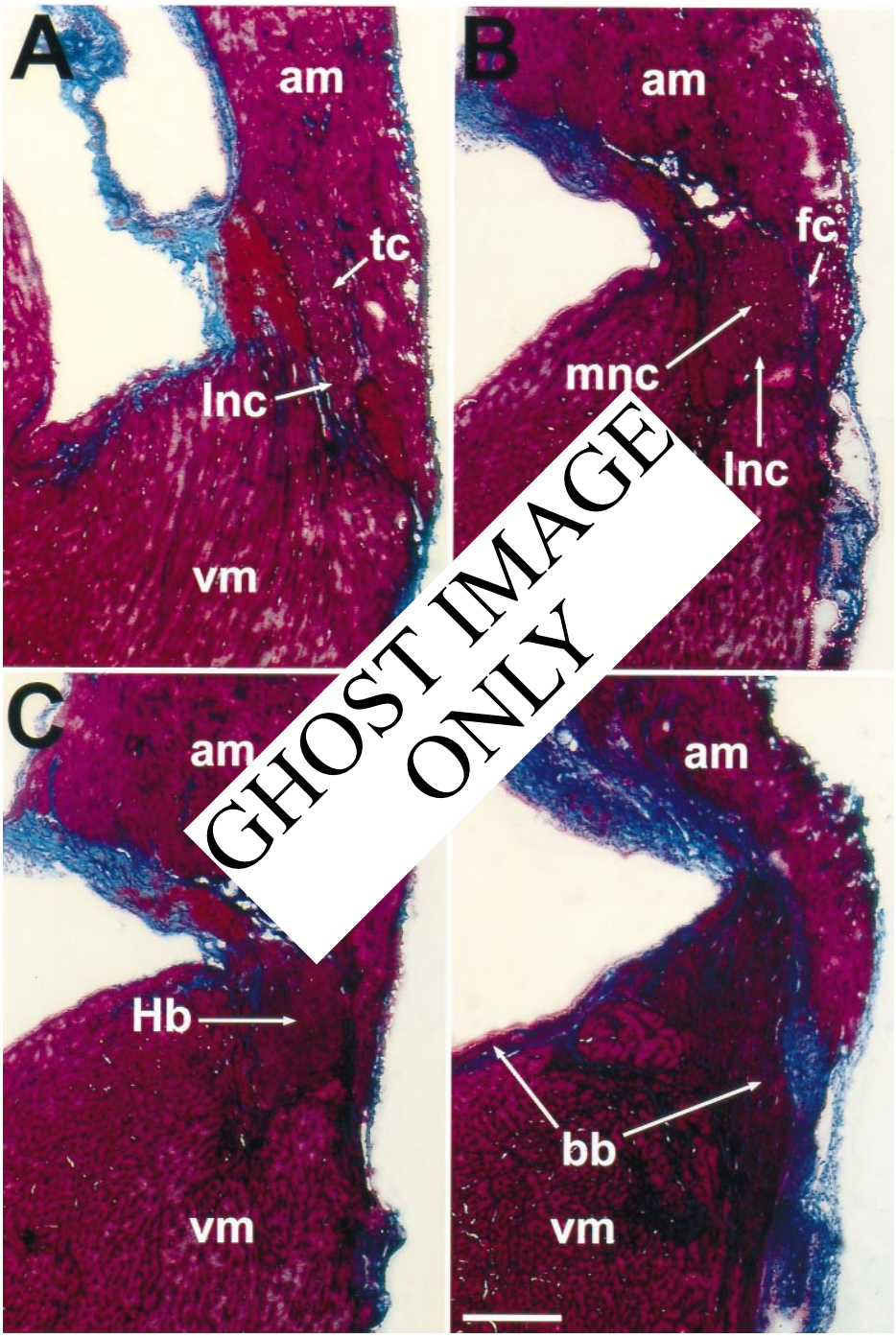

Fig. 1. Sections in the frontal plane tracing the course of the rat AV node, His bundle and bundle branches from posterior to anterior. Red staining indicates myocardial cells and blue staining indicates collagen. (*A*) Section taken through the open node. (*B*) Section taken through the junction of the open and enclosed node. (*C*) Section taken through the His bundle. (*D*) Section taken through the left and right bundle branches. Am, atrial myocardium; vm, ventricular myocardium; tc, transitional cell region; lnc, lower nodal cells; fc, fibrous capsule; mnc, midnodal cell region; Hb, His bundle; bb, bundle branches. Bar, 250 μm.

septum with the inferior border at the attachment of the septal tricuspid leaflet. The node is divided into 2 parts, a posterior open region (Fig. 1*a*) and an anterior enclosed region (Fig. 1*b*). These 2 regions are separated by a fibrous collar which encircles the anterior portion of the node. The anterior enclosed node, originally described as part of the penetrating AV bundle by Tawara (1906), is directly continuous with the His bundle which passes superficially on the right side of the central fibrous body before turning into the annulus fibrosus and penetrating it to reach the ventricular septum forming the bundle branches

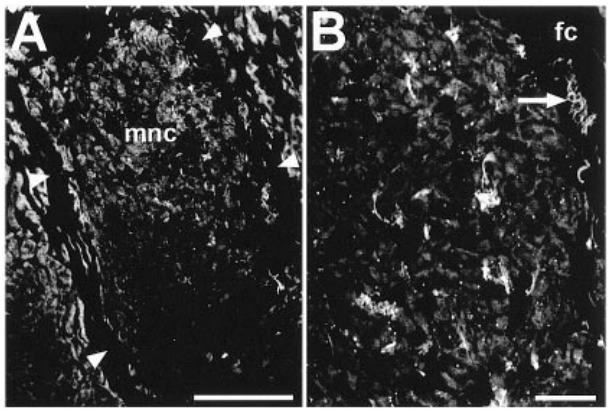

Fig. 2. Low and high magnification confocal images of PGP 9.5-immunoreactivity throughout the rat midnodal cell region. (*A*) Midnodal cell region. Arrowheads delineate the fibrous capsule surrounding the midnodal cell region. (*B*) Midnodal cell region. Arrow indicates a nerve tract. mnc, midnodal cell region; fc, fibrous capsule. Bars: (*A*) 125 μm, (*B*) 30 μm.

(Fig. 1*c*, *d*). The posterior open node is a much larger area with its deep boundary being formed by the annulus fibrosus thereby separating it from the ventricular septum. Superficially, the posterior open node is continuous with the atrial myocardium (Fig. 1*a*).

In agreement with previous findings in rat (Mochet et al. 1975) and rabbit (Anderson, 1972), we were able to discern that the AV nodal region contains cells that can be delineated into distinct cellular zones. Differentiation of these cellular zones was clearest when the specimen was sectioned in the frontal plane. Within the AV node 3 different cell types could be distinguished. Transitional, or AN, cells were found for the most part in the open node (Fig. 1*a*). They were intermediate in morphology between atrial cells and other nodal cells and were arranged in a parallel fashion separated from neighbouring cells by connective tissue. Having entered the anterior enclosed node, some of these cells retained their transitional characteristics and passed circumferentially inside the fibrous collar forming the circumferential transitional cell layer. The more centrally located transitional cells merged together to form a knot of tightly packed spherical cells at the entrance of the anterior enclosed node. These cells corresponded to midnodal, or N cells (Fig. 1*b*). Running in parallel with the annulus fibrosus was a tract of cells called lower nodal, or NH, cells (Fig. 1*a*, *b*). These cells occupied the lower portion of the anterior enclosed node and were larger than the transitional or midnodal cells. When traced anteriorly, the bundle of lower nodal cells expanded rapidly to form the His bundle (Fig. 1*c*). The lower nodal cell tract could also be traced in the posterior direction where it passes underneath the ostium of the coronary sinus.

Innervation

The entire AV nodal region, the His bundle and the bundle branches exhibited a rich nerve supply as visualised by immunoreactivity for the general neuronal marker PGP 9.5. Low and high magnification confocal microscope images revealed that PGP 9.5-immunoreactivity is observed in a spatially uniform manner throughout the midnodal cell region (Fig. 2*a*, *b*).

AChE-reactivity was used as a marker for parasympathetic innervation. Our results revealed that all regions of the AV node and ventricular conduction system receive a denser parasympathetic innervation than the atrial or the ventricular myocardium (Fig. 3*a–f*). However, the spatial distribution of nerve processes throughout the AV nodal region was not uniform. Abundant AChE-reactive nerve processes were found throughout the transitional cell region with a preponderance of nerve processes found in the lower nodal cell tract (Fig. 3*a*, arrow) while the circumferential transitional cell region, that envelops the midnodal cell region, also showed a preponderance of AChE-reactive nerve processes (Fig. 3*b*, arrows). In contrast, the central midnodal cell region demonstrated a paucity of AChE-reactivity (Fig. 3*b*, asterisk). The lower nodal cell tract was also heavily AChE reactive (Fig. 3*b*). The ventricular conduction system, similar to the transitional cell region, demonstrated an abundance of AChE-reactive nerve processes (Fig. 3*c*, *d*). In addition, the atrial myocardium contained more AChE-reactive nerve processes than the ventricular myocardium (Fig. 3*e*, *f*).

Low and high magnification confocal microscope images revealed that TH-immunoreactivity is observed in the transitional and midnodal cell regions and the ventricular conduction system (Fig. 4*a–f*). TH-immunoreactive nerve processes were present throughout the AV node and bundle branches in a spatially uniform pattern with the amount of immunoreactive nerve processes being greatest in the transitional cell region (Fig. 4*a*, *b*), less in the midnodal cell region (Fig. 4*c*, *d*) and least in the ventricular conduction system (Fig. 4*e*, *f*). Moreover, the amount of TH-immunoreactive nerve processes in all regions of the AV conduction system were greater than in the atrial and ventricular myocardium (Fig. 4*a–f*).

Confocal images revealed that VIP and CGRP immunoreactivity was not detectable in any region of

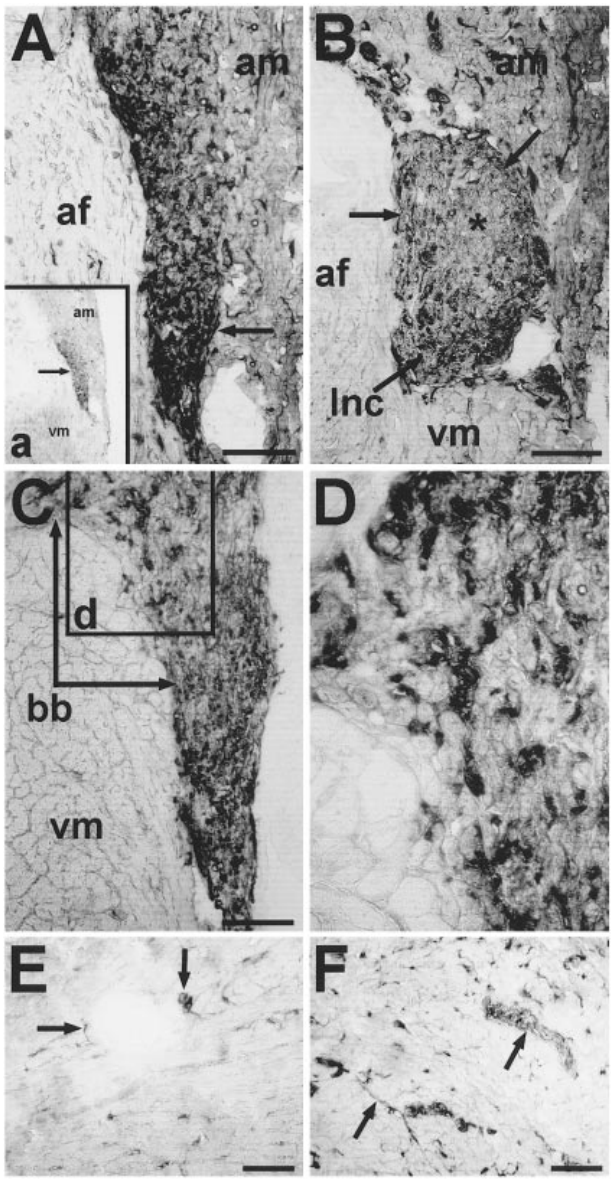

Fig. 3. AChE-reactivity in the AV node and ventricular conduction system. (*A*) AChE-reactivity in the transitional cell region. Arrow indicates the lower nodal cell region. (*a*) Low magnification view of region in *A*. Arrow indicates the transitional cell region. (*B*) AChE-reactivity in the midnodal cell region. Asterisk indicates the central midnodal cell region. Arrows indicate the circumferential transitional cell region. (*C*) AChE-reactivity in the bundle branches. (*D*) High magnification view of region in *d*. (*E*) AChE-reactivity in the ventricular myocardium. Arrows indicate AChE-reactive nerve processes adjacent to a blood vessel. (*F*) AChE-reactivity in the atrial myocardium. Upper arrow indicates an AChE-reactive nerve tract, lower arrow indicates an AChE-reactive nerve. am, atrial myocardium; af, annulus fibrosus; lnc, lower nodal cells; bb, bundle branch; vm, ventricular myocardium. Bars: *A*, *B*, *C*, 125 μm; *E*, *F*, 45 μm.

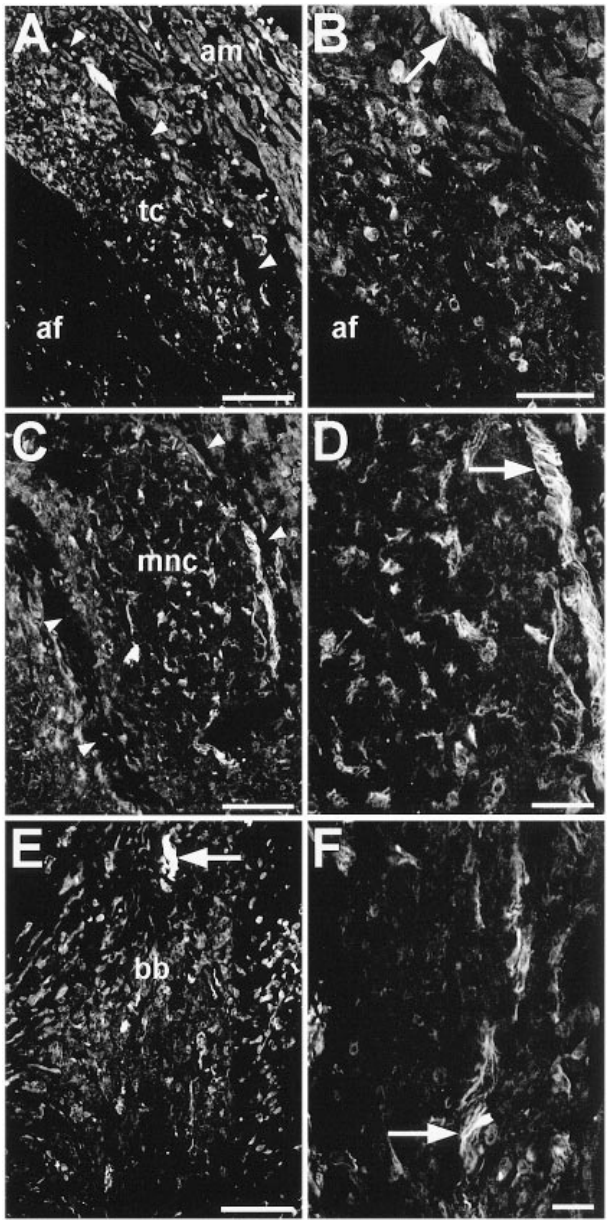

Fig. 4. Low and high magnification confocal images of TH immunoreactivity throughout the rat AV node. (*A*) Transitional cell region. Arrowheads delineate the transitional cell region from the atrial myocardium. (*B*) Transitional cell region. Arrow indicates a nerve tract. (*C*) Midnodal cell region. Arrowheads delineate the fibrous capsule surrounding the midnodal cell region. (*D*) Midnodal cell region. Arrow indicates a nerve tract. (*E*) Bundle branch. Arrow indicates a nerve tract. (*F*) Bundle branch. Arrow indicates a nerve fibre. am, atrial myocardium; tc, transitional cell region; af, annulus fibrosus; mnc, midnodal cell region; bb, branching bundle. Bars: *A*, *C*, *E*, 90 μm; *B*, *D*, 25 μm; *F*, 20 μm.

the rat AV node, His bundle or bundle branches (Fig. 5*a–f*). This lack of detection was not due to a lack of specificity for either the anti-VIP or anti-CGRP antibodies to their corresponding antigens in the rat heart as VIP and CGRP-immunoreactive nerve processes could be localised in the walls of blood vessels in the rat heart (Fig. 5*g*, *h*, respectively).

β_1- *and* β_2-*adrenoreceptors*

β_1-AR immunoreactivity was present in all regions of the AV node and ventricular conduction system (Fig.

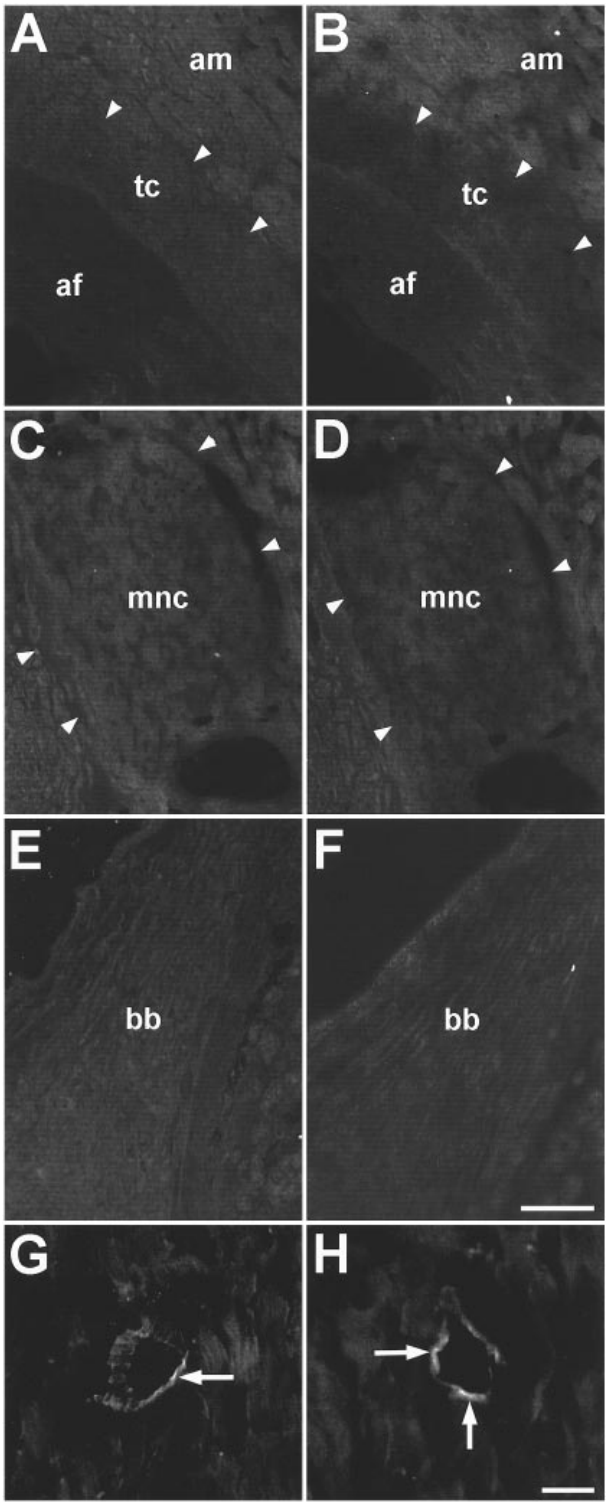

Fig. 5. Confocal images of VIP and CGRP-immunoreactivity throughout the rat AV node. (*A*) VIP immunoreactivity in the transitional cell region. Arrowheads delineate the transitional cell region from the atrial myocardium. (*B*) CGRP immunoreactivity in the transitional cell region. Arrowheads delineate the transitional cell region from the atrial myocardium. (*C*) VIP immunoreactivity in the midnodal cell region. Arrowheads delineate the fibrous capsule surrounding the midnodal cell region. (*D*) CGRP immunoreactivity in the midnodal cell region. Arrowheads delineate the fibrous capsule surrounding the midnodal cell region. (*E*) VIP immunoreactivity in the bundle branch. (*F*) CGRP immunoreactivity in the bundle branch. (*G*) VIP immunoreactivity in a blood vessel wall. (*H*) CGRP immunoreactivity in a blood vessel wall. am, atrial myocardium; tc, transitional cell region; af, annulus fibrosus; mnc, midnodal cell region; bb, bundle branch. Magnification in *A–F* is the same; magnification in *G* and *H* is the same. Bars: *F*, 90 μm, *H*, 45 μm.

6*a–c*). Low magnification confocal images revealed that the level of β_1-AR immunoreactivity was similar in the atrial myocardium and transitional cell region (Fig. 6*a*, arrowheads delineate the transitional cell region). Furthermore, the spatial distribution appeared to be nonuniform throughout the midnodal cell region with a predominance of β_1-AR immunoreactivity in the circumferential transitional cell layer (Fig. 6*b*, arrow). β_1-AR immunoreactivity was uniformly distributed in the bundle branches (Fig. 6*c*). Similar to the β_1-AR, β_2-AR immunoreactivity was also present in the transitional and midnodal cell regions of the AV node (Fig. 6*e*, *f*). However, unlike the β_1-AR, β_2-AR immunoreactivity was not detectable in the atrial myocardium (Fig. 6*e*). Moreover, the spatial distribution of β_2-AR immunoreactivity in the midnodal cell region was nonuniform. The central midnodal cell region exhibited β_2-AR immunoreactivity while the peripheral midnodal cell region, corresponding to the circumferential transitional cell layer, did not appear to exhibit any detectable β_2-AR immunoreactivity (Fig. 6*f*, asterisk indicates the circumferential transitional cell layer). Furthermore, the bundle branches expressed high levels of β_2-AR immunoreactivity (Fig. 6*g*). Finally, it was demonstrated that both β_1-ARs and β_2-ARs can be localised to nerve processes, in addition to cardiac myocytes, in the AV and ventricular conduction system (Fig. 6*d*, *h*).

DISCUSSION

This study demonstrates, as in other species (Anderson, 1972; Crick et al. 1994, 1996*a*, *b*), that the rat AV node, His bundle and bundle branches are more densely innervated than the atrial or ventricular myocardium. This is as expected considering the role of the ANS in regulating AV conduction. In this study, the total innervation pattern of the rat AV node, His bundle and bundle branches was determined using antiserum for the general neuronal marker PGP 9.5. Our results demonstrate that the transitional cell region is the most densely innervated region of the AV and ventricular conduction systems in the rat heart followed by the midnodal cell region and the ventricular conduction tissues. This pattern of general innervation distribution is similar to what has been reported in other species including man (Crick et al.

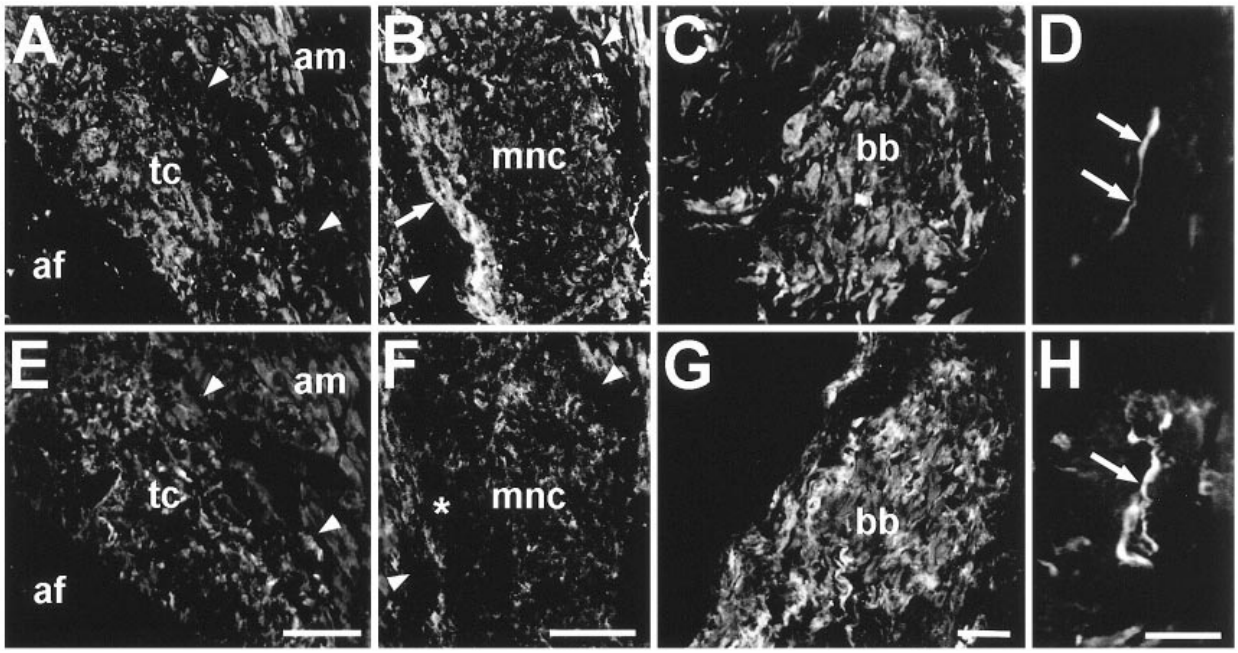

Fig. 6. Confocal images of β_1-AR and β_2-AR immunoreactivity throughout the rat AV node. (*A*) β_1-AR immunoreactivity in the transitional cell region. Arrowheads delineate the transitional cell region from the atrial myocardium. (*B*) β_1-AR immunoreactivity in the midnodal cell region. Arrow demarcates the circumferential transitional cell layer. Arrowheads delineate the fibrous capsule surrounding the midnodal cell region. (*C*) β_1-AR immunoreactivity in the bundle branch. (*D*) β_1-AR immunoreactivity of a nerve fibre. (*E*) β_2-AR immunoreactivity in the transitional cell region. Arrowheads delineate the transitional cell region from the atrial myocardium. (*F*) β_2-AR immunoreactivity in the midnodal cell region. Asterisk demarcates the circumferential transitional cell layer. Arrowheads delineate the fibrous capsule surrounding the midnodal cell region. (*G*) β_2-AR immunoreactivity in the bundle branch. (*H*) β_2-AR immunoreactivity of a nerve fibre. am, atrial myocardium; tc, transitional cell region; af, annulus fibrosus; mnc, midnodal cell region; bb, bundle branch. Bars: *A*, *E*, 75 μm, *B*, *F*, 90 μm, *C*, *G*, 40 μm, *D*, *H*, 10 μm.

1994) and calf (Crick et al. 1996*b*) hearts. What is of specific interest to note in this study is the uniform spatial distribution of all populations of nerve processes within the midnodal cell region.

The innervation supplied by the parasympathetic branch of the ANS was determined by visualising AChE reactivity. In this study in the rat, our results demonstrate a preponderance of AChE-reactive nerve processes in the transitional cell region. This finding is in agreement with reports in human (Crick et al. 1994) and calf (Crick et al. 1996*b*) hearts. Furthermore, we found a paucity AChE-reactive nerve processes in the central midnodal cell region and an abundance of AChE-reactive nerve processes localised in the circumferential transitional cell layer. Using a similar technique, Anderson (1972) demonstrated a similar nonuniform distribution of AChE reactivity within the rabbit AV node, suggesting a nonuniform density of AChE-reactive nerve processes. In contrast, Imaizumi et al. (1990) reported a preponderance of AChE reactivity throughout the midnodal cell region of the rabbit. In 9 rabbit AV nodes examined we observed a differential spatial distribution of AChE-reactive nerve processes with a preponderance of nerve processes found in the circumferential transitional cell layer and a paucity in the central midnodal cell region (unpublished observations).

The sympathetic division of the ANS was visualised using an antibody directed against TH. Our results demonstrate the presence of an extensive population of TH-immunoreactive nerve tracts running through the AV and ventricular conduction systems, and nerve fibres interspersed between myocytes, indicating that the sympathetic nervous system is poised to exert a powerful influence on AV conduction time. Similar findings have been reported in the hearts of other species including human (Crick et al. 1994), guinea pig (Crick et al. 1996*a*) and calf (Crick et al. 1996*b*) hearts. We found that TH immunoreactivity is greatest in the transitional cell region with decreasing levels of immunoreactivity in the midnodal cell region and the ventricular conduction tissues. More specifically, and in contrast to the spatial distribution of AChE-reactive nerve processes, the spatial distribution of TH-immunoreactive nerve processes in the circumferential transitional cell layer and midnodal cell region was found to be uniform.

Thus the uniform pattern of total innervation that

was visualised using PGP 9.5 represents the combination of at least 2 subpopulations of nerves, with each division of the ANS displaying a different pattern of spatial distribution within the midnodal cell region.

Autonomic interactions in the heart have been reported to occur at both prejunctional and postjunctional levels (Levy, 1995). At the postjunctional level, the interaction of the sympathetic and parasympathetic branches is manifested through adenyl cyclase, with sympathetic activity increasing intracellular cAMP levels and parasympathetic activity attenuating this increase by inhibiting adenyl cyclase (Levy, 1995). Of more direct relevance to this study is the interaction that takes place at the prejunctional level. Muscarinic receptors located on postganglionic sympathetic nerve endings inhibit the release of NA, whereas NA acts to inhibit the release of ACh from parasympathetic nerve endings (Levy, 1995). When the effects of combined autonomic interactions on the AV junction are considered it has been demonstrated that there is a significant sympathetic-parasympathetic interaction in the control of AV conduction in the dog heart (Urthaler et al. 1986). The nature and extent of this interaction, however, is very different from that observed in the sinus node. Whereas for the regulation of the sinus rate, accentuated antagonism with parasympathetic predominance is the characteristic mode of action of the ANS, the reverse is true for the control of AV conduction. The accentuated antagonism that regulates AV conduction shows a clear predominance of sympathetic activity over parasympathetic restraint (Urthaler et al. 1986). It has been hypothesised that the observed sympathetic preponderance over vagal activity on AV conduction might be due to greater distance between the sympathetic and parasympathetic nerve endings or perhaps due to fewer or even a lack of muscarinic receptors in a large number of sympathetic nerve terminals in the AV junction (Urthaler et al. 1986). The results from the present study indicate that there may be some validity to this hypothesis since, within the midnodal cell region, there is little overlap of the 2 subpopulations of the ANS, with only the circumferential transitional cell layer being innervated by both parasympathetic and sympathetic branches of the ANS.

In addition to the presence of the classical neurotransmitters, NA and ACh, subpopulations of autonomic and sensory cardiac nerves also contain immunohistochemically defined neuropeptides, such as VIP, CGRP and NPY, which elicit variable effects on cardiovascular function (Fisher et al. 1983; Rigel, 1988; Rigel & Lathrop, 1990; Levy 1995).

Our results demonstrate that CGRP immunoreactivity is not detectable in the rat AV node, His bundle or bundle branches, leading one to speculate that CGRP is not involved in the neural regulation of AV conduction time in the rat. Similarly, it has been reported that a sparse amount of CGRP immunoreactivity was found in bovine (Forsgren, 1994), human (Crick et al. 1994) and dog (Ursell et al. 1991*a*, *b*) AV and ventricular conduction systems. In contrast, a rich supply of CGRP-immunoreactive neural elements was reported to be found in the guinea pig (Crick et al. 1996*a*) and calf (Crick et al. 1996*b*) AV and ventricular conduction systems. In agreement with other reports (Mulderry et al. 1985; Forsgren, 1994; Ursell et al. 1991*a*, *b*), we found that CGRP immunoreactivity was localised to nerve processes in blood vessel walls.

The great majority of CGRP immunoreactive neural tissue has been localised to the SA nodal region in dog (Ursell et al. 1991*a*, *b*), bovine (Forsgren, 1994), guinea pig (Steele & Choate, 1994; Crick et al. 1996*a*) and human (Crick et al. 1994) hearts.

As with CGRP immunoreactivity, we found no detectable VIP immunoreactivity in the rat AV and ventricular conduction systems. Similar results have been reported in the AV and ventricular conduction systems of other species. In calf hearts, low levels of VIP were detected in the transitional cell region, whereas VIP was not detected in the midnodal cell region or ventricular conduction tissues (Crick et al. 1996*b*). In the guinea pig, sparse VIP immunoreactivity was found in the ventricular conduction system, but none was detected in the AV node (Crick et al. 1996*a*). In humans, sparse VIP was detectable in the ventricular conduction tissues, but none was detectable in the AV node with the exception of blood vessel walls (Crick et al. 1994), as in this study.

VIP has been demonstrated to coexist with ACh in postganglionic parasympathetic neurons (Forssmann et al. 1988). It has been reported to have coronary vasodilatory effects in rabbit (Accili et al. 1995), and inotropic (Anderson et al. 1988), chronotropic (Rigel, 1988; Hill et al. 1993) and dromotropic effects (Rigel & Lathrop, 1990) in dog. Similar to CGRP localisation, it has been reported that VIP-containing neural elements are predominantly localised in the SA node (Weihe et al. 1984; Steele & Choate, 1994).

Our results demonstrate a preponderance of β_1 and β_2-ARs throughout the AV node, His bundle, and bundle branches in the rat heart. β_1-AR immunoreactivity was not confined to these conduction tissues but was also found in the working myocardium. In contrast, β_2-AR immunoreactivity was confined to

these conduction tissues. It is of importance to point out that while β_1-ARs exhibited a uniform spatial distribution in the midnodal and circumferential transitional cell regions, β_2-ARs did not. While abundant β_2-ARs were found in the central midnodal cell region, the circumferential transitional cell layer that envelopes this midnodal cell region exhibited a paucity of β_2-AR expression. The present study, however, does not allow for the determination of specific cellular localisation of these β-ARs. These sites could be predominantly localised post-synaptically on specialised cells belonging to the AV and ventricular conduction system. Our results do, however, demonstrate that both of these β-ARs can be localised to nerve fibres. A similar finding regarding β_2-AR localisation to nerve fibres has been reported in guinea pig heart (Haberberger & Kummer, 1996).

The coexistence of β_1 and β_2-ARs in the AV conduction system in the rat (Saito et al. 1988) and guinea pig (Molenaar et al. 1990) heart has been reported using autoradiographic techniques, but it is not possible to determine their precise localisation in the various nodal regions from these reports. In addition to the AV node, the coexistence of β_1 and β_2-ARs has been reported in the rat (Saito et al. 1989), human (Rodefeld et al. 1996) and dog (Beau et al. 1995) SA nodes.

β_1-ARs have been proposed to preferentially mediate responses to neuronally released NA, whereas β_2-ARs have been proposed to preferentially mediate responses to circulating adrenaline (Lands et al. 1967). Interestingly, it has been reported that the denervated transplanted heart retains the ability to significantly shorten the P-R interval on exercise (Koller-Strametz et al. 1997). Since the transplanted heart remains extrinsically denervated indefinitely, and thus sympathetic nerve activity has no influence on conduction, circulating catecholamines are a possible cause of the enhancement of AV nodal conduction on exercise. Thus the dynamic exercise induced changes in P-R interval in the transplanted heart may be explained by an increase in circulating plasma catecholamines eliciting their effect through β_2-adrenoreceptors (Koller-Strametz et al. 1997). Moreover, the β_2-AR, in addition to the β_1-AR, has been shown to have positive dromotropic effects in dog heart (Takei et al. 1992).

The finding that the midnodal cell region exhibits a paucity of AChE-reactive nerve processes while the circumferential transitional cell layer, that envelopes the midnodal cell region, exhibits an abundance of these nerve processes, indicates that the parasympathetic branch of the ANS is potentially exerting its influence on AV conduction time in specific regions of the AV node. It is possible that this influence is taking place only in the transitional, circumferential transitional or lower nodal cell regions, or in any combination of these 3 regions, and not in the central midnodal cell region directly. The finding that TH immunoreactivity is present throughout the transitional, lower nodal, midnodal and circumferential transitional cell regions in a spatially uniform manner indicates that the sympathetic division of the ANS could potentially exert its influence on AV conduction at any of these AV nodal regions.

In addition to the spatial heterogeneity of the parasympathetic division of the ANS and β-ARs described in this study, an additional spatial heterogeneity in the distribution of the fast inward sodium current (Munk et al. 1996), sodium channel protein expression (Petrecca et al. 1997), and connexin 43-containing gap junction protein expression (Petrecca et al. 1997) has been reported. An electrophysiological survey of cells isolated from specific regions of the rabbit AV node described populations of cells that exhibit distinct action potential configurations as well as different profiles in the distribution and magnitude of sodium and other ionic currents (Munk et al. 1996). Also, immunohistochemical investigations have demonstrated a nonuniform pattern of sodium channel protein expression in the AV node of the rabbit (Petrecca et al. 1997). The results indicate a paucity of sodium channel protein expression in the central midnodal cell region of the rabbit AV node while the transitional, circumferential transitional and lower nodal cell regions all contain levels of sodium channel protein expression that are similar to that of the adjacent working myocardium. The spatial distribution of connexin 43-containing gap junctions has also been reported to be strikingly similar to that of sodium channels (Petrecca et al. 1997). Of key importance in these studies is that the circumferential transitional cells retain relatively high levels of both sodium channel and connexin 43 protein expression, whereas the central midnodal cell region exhibits relatively weak expression. This leads to the speculation that impulse conduction would be favoured in the circumferential transitional cell envelope with the midnodal cell region acting as an electrical sink for current flow.

This proposed preferential pathway for impulse conduction through the circumferential transitional cell envelope could then be influenced by the parasympathetic division of the ANS, which is predominantly localised in this region and remarkably

absent in the central midnodal cell region. In contrast, the sympathetic branch of the ANS is generously supplied in a uniform manner throughout the node. Since the central midnodal cell region has been reported to display a calcium-dependent, and not a fast inward sodium current, upstroke (Hoffman, 1961; Zipes & Mendez, 1973; Anderson et al. 1974; Wit & Cranefield, 1974; Akiyama & Fozzard, 1979; Noma et al. 1980; Watanabe, 1981; Mendez, 1982; Munk et al. 1996), sympathetic nervous stimulation would tend to increase the calcium-dependent upstroke velocity in this region (Marban & O'Rourke, 1995). The other regions of the AV node which do express sodium channels would not necessarily exhibit an increase in upstroke velocity since their upstrokes are sodium dependent. Thus the midnodal cell region, which in the absence of neuromodulation could be acting as an electrical sink drawing current flow from the impulse as it passes around the midnodal region in the circumferential transitional cell envelope could, on sympathetic stimulation, either become less of a sink or may even begin to act as a source, thus decreasing the current drain from the impulse as it passes around the midnodal region leading to a decrease in conduction time. Parasympathetic modulation, on the other hand, could be taking place in the transitional, circumferential transitional or lower nodal cell regions.

Thus the observation that the midnodal cell region exhibits a differential spatial pattern of parasympathetic and sympathetic innervation suggests a preferential pathway for impulse conduction through this region. Moreover, the localisation of β_2-ARs in the AV conduction system suggests that subtype-specific pharmacological agents may be useful in influencing AV nodal conduction time. Subsequent studies that combine optical imaging with histological and immunohistochemical techniques will be required to further characterise impulse conduction through the AV nodal region and the contribution of the ANS at specific sites within this region and its influence on AV nodal conduction time.

ACKNOWLEDGEMENTS

The authors wish to acknowledge the technical assistance of Johanne Ouellette. Special thanks are due to Dr S. A. Cohen for thoughtful discussions and careful review of the manuscript. This research was supported by a grant to A. Shrier from the Medical Research Council of Canada. K. Petrecca is supported by a studentship from the Fonds pour la Formation de Chercheurs et l'Aide à la Recherche.

REFERENCES

Accili EA, Buchan AMJ, Kwok YN, Ledsome JR, Brown JC (1995) Presence and actions of vasoactive intestinal peptide in the isolated rabbit heart. *Canadian Journal of Physiology and Pharmacology* **73**, 134–139.

Akiyama T, Fozzard HA (1979) Ca and Na selectivity of the active membrane of rabbit AV nodal cells. *American Journal of Physiology* **236**, C1–C8.

Anderson FL, Kralios AC, Hershberger R, Bristow MR (1988) Effect of vasoactive intestinal peptide on myocardial contractility and coronary blood flow in dog: comparison with isoproterenol and forskolin. *Journal of Cardiovascular Pharmacology* **12**, 365–371.

Anderson RH (1972) Histological and histochemical evidence concerning the presence of morphologically distinct cellular zones within the rabbit atrioventricular node. *Anatomical Record* **173**, 7–23.

Anderson RH, Janse MJ, Van Capelle FJL, Billette J, Becker AE, Durrer D (1974) A combined morphological and electrophysiological study of the atrioventricular node of the rabbit heart. *Circulation Research* **35**, 909–922.

Beau SL, Hand DE, Schuessler RB, Bromberg BI, Kwon B, Boineau JP et al. (1995) Relative densities of muscarinic cholinergic and β-adrenergic receptors in the canine sinoatrial node and the relation to sites of pacemaker activity. *Circulation Research* **77**, 957–963.

Billette J (1987) Atrioventricular nodal activation during periodic premature stimulation of the atrium. *American Journal of Physiology* **252**, 163–177.

Cowen T, Haven AJ, Burnstock G (1985) Pontamine sky blue: a counterstain for background autofluorescence in fluorescence and immunofluorescence histochemistry. *Histochemistry* **82**, 205–208.

Crick SJ, Wharton J, Sheppard MN, Royston D, Yacoub MH, Anderson RH, et al. (1994) Innervation of the human cardiac conduction system. A quantitative immunohistochemical and histochemical study. *Circulation* **89**, 1697–1708.

Crick SJ, Sheppard MN, Anderson RH, Polak JM, Wharton J (1996*a*) A quantitative study of nerve distribution in the conduction system of the guinea pig heart. *Journal of Anatomy* **188**, 403–416.

Crick SJ, Sheppard MN, Anderson RH, Polak JM, Wharton J (1996*b*) A quantitative assessment of innervation in the conduction system of the calf heart. *Anatomical Record* **245**, 685–698.

El-Badawi A, Schenk EA (1967) Histochemical methods for separate, consecutive and simultaneous demonstration of acetylcholinesterase and norepinephrine in cryostat section. *Journal of Histochemistry and Cytochemistry* **15**, 580–588.

Fisher LA, Kikkawa DO, Rivier JE, Amara SG, Evans RM, Rosenfeld MG et al. (1983) Stimulation of noradrenergic sympathetic outflow by calcitonin gene-related peptide. *Nature* **305**, 534–536.

Forsgren S (1994) Distribution of calcitonin gene-related peptide-like immunoreactivity in the bovine conduction system: correlation with substance P. *Regulatory Peptides* **52**, 7–19.

Forssmann WG, Triepel J, Daffner C, Heym CH, Cuevas P, Nobel MIM et al. (1988) Vasoactive intestinal peptide in the heart. *Annals of the New York Academy of Sciences* **527**, 405–420.

Haberberger R, Kummer W (1996) β2-Adrenoreceptor immunoreactivity in cardiac ganglia of the guinea pig. *Histochemical Journal* **28**, 827–833.

Hill MRS, Wallick DW, Martin PJ, Levy MN (1993) Frequency dependence of vasoactive intestinal polypeptide release and vagally induced tachycardia in the canine heart. *Journal of the Autonomic Nervous System* **43**, 117–122.

Hoffman VF (1961) Physiology of atrioventricular transmission. *Circulation* **24**, 506–517.

Hoffman BF (1967) Autonomic control of cardiac rhythm. *Bulletin of the New York Academy of Medicine* **43**, 1087–1096.

Imaizumi S, Mazgalev T, Dreifus LS, Michelson EL, Miyagawa A, Bharati et al. (1990) Morphological and electrophysiological correlates of the atrioventricular nodal response to increased vagal activity. *Circulation* **82**, 951–964.

Koller-Strametz J, Kratochwill C, Grabenwoger M, Laufer G, Pacher R, Gemeiner N et al. (1997) PR interval adaptation in the denervated transplanted heart. *Pacing and Clinical Electrophysiology* **20**, 1247–1251.

Lands AM, Arnold A, McAuliff JP, Ludena FP, Brown TG (1967) Differentiation of receptor systems activated by sympathomimetic amines. *Nature* **214**, 597–598.

Levy MN (1995) Time dependency of the autonomic interactions that regulate heart rate and rhythm. In *Cardiac Electrophysiology: from Cell to Bedside* (ed. Zipes DP, Jalife J), pp. 454–459. Philadelphia: W. B. Saunders.

Levy MN, Martin PJ (1979) Neural control of the heart. In *Handbook of Physiology* (ed. Berne RM), pp. 581–620. Maryland: Bethesda, American Physiological Society.

Marban E, O'Rourke B (1995) Calcium channels: structure, function, and regulation. In *Cardiac Electrophysiology: from Cell To Bedside* (ed. Zipes DP, Jalife J), pp. 11–21. Philadelphia: W. B. Saunders.

Mendez C (1982) Characteristics of impulse propagation in the mammalian atrioventricular node. In *Normal and Abnormal Conduction in the Heart* (ed. Paes de Carvalho A, Hoffman BF, Lieberman M), pp. 363–377. New York: Futura.

Mochet M, Moravec J, Guillemot H, Hyatt PY (1975) The ultrastructure of rat conductive tissue: an electron microscopic study of the atrioventricular node and bundle of His. *Journal of Molecular and Cellular Cardiology* **7**, 879–889.

Molenaar P, Russell FD, Shimada T, Summers RJ (1990) Densitometric analysis of β1- and β2-adrenoreceptors in guinea-pig atrioventricular conducting system. *Journal of Molecular and Cellular Cardiology* **22**, 483–495.

Mulderry PK, Ghatei MA, Rodrigo J, Allen JM, Rosenfeld MG, Polak et al. (1985) Calcitonin gene-related peptide in cardiovascular tissues of the rat heart. *Neuroscience* **14**, 947–954.

Munk AA, Adjemian RA, Zhao J, Ogbaghebriel A, Shrier A (1996) Electrophysiological properties of morphologically distinct cells isolated from the rabbit atrioventricular node. *Journal of Physiology* **493**, 801–818.

Noma A, Irisawa H, Kokobun S, Kotake H, Nishimura M, Watanabe Y (1980) Slow current systems in the A–V node of the rabbit heart. *Nature* **285**, 228–229.

Paes de Carvalho A, Almeida DF (1960) Spread of activity through the atrioventricular node. *Circulation Research* **8**, 801–809.

Petrecca K, Amellal F, Laird DW, Cohen SA, Shrier A (1997) Sodium channel distribution within the rabbit AV node and surrounding myocardium as analysed by confocal microscopy. *Journal of Physiology* **501**, 263–274.

Rigel DF (1988) Effects of neuropeptides on heart rate in dog: comparison of VIP, PHI, NPY, CGRP, and NT. *American Journal of Physiology* **255**, H311–H317.

Rigel DF, Lathrop DA (1990) Vasoactive intestinal polypeptide facilitates atrioventricular nodal conduction and shortens atrial and ventricular refractory periods in conscious and anesthetized dogs. *Circulation Research* **67**, 1323–1333.

Rodefeld MD, Beau SL, Schuessler RB, Boineau JP, Saffitz JE (1996) β-Adrenergic and muscarinic cholinergic receptor densities in the human sinoatrial node: identification of a high β_2-adrenoreceptor density. *Journal of Cardiovascular Electrophysiology* **7**, 1039–1049.

Saito K, Kurihara M, Cruciani R, Potter WZ, Saavedra JM (1988) Characterization of β_1- and β_2-adrenoreceptor subtypes in the rat atrioventricular node by quantitative autoradiography. *Circulation Research* **62**, 173–177.

Saito K, Torda T, Potter WZ, Saavedra JM (1989) Characterization of β_1- and β_2-adrenoreceptor subtypes in the rat sinoatrial node and stellate ganglia by quantitative autoradiography. *Neuroscience Letters* **96**, 35–41.

Steele PA, Choate JK (1994) Innervation of the pacemaker in guinea-pig sinoatrial node. *Journal of the Autonomic Nervous System* **47**, 177–187.

Takei M, Furukawa Y, Narita M, Murakami M, Ren LM, Karasawa Y et al. (1992) Sympathetic nerve stimulation activates both β_1 and β_2-adrenoreceptors of SA and AV nodes in anesthetized dogs. *Japanese Journal of Pharmacology* **59**, 23–30.

Tawara S (1906) *Das Reizleitungssystem des Saugetierherzens*. Jena: G. Fischer.

Ursell PC, Ren CL, Danilo Jr P (1991*a*) Anatomic distribution of autonomic neural tissue in the developing dog heart: II. Nonadrenergic noncholinergic innervation by calcitonin gene-related peptide-immunoreactive tissue. *Anatomical Record* **230**, 531–538.

Ursell PC, Ren CL, Albala A, Danilo Jr P. (1991*b*) Non-adrenergic noncholinergic innervation. Anatomic distribution of calcitonin gene-related peptide-immunoreactive tissue in the dog heart. *Circulation Research* **68**, 131–140.

Urthaler F, Neely BH, Hageman GR, Smith LR (1986) Differential sympathetic-parasympathetic interactions of sinus node and AV junction. *American Journal of Physiology* **250**, H43–H51.

Watanabe Y (1981) Peculiarities of AV nodal conduction and the role of slow Na current. *Japanese Circulation Journal* **45**, 446–452.

Weihe E, Reinecke M, Forssmann WG (1984) Distribution of vasoactive intestinal polypeptide-like immunoreactivity in the mammalian heart. *Cell and Tissue Research* **236**, 527–540.

Wit AL, Cranefield PF (1974) Effect of verapamil on the sinoatrial and atrioventricular nodes of the rabbit and the mechanism by which it arrests reentrant atrioventricular tachycardia. *Circulation Research* **35**, 413–425.

Zipes DP, Mendez C (1973) Action of manganese ions and tetrodotoxin on atrioventricular nodal transmembrane potentials in isolated rabbit hearts. *Circulation Research* **32**, 447–454.